Instanton-Induced Processes
An Overview

F. Schrempp
Deutsches Elektronen-Synchrotron DESY, Hamburg, Germany

Abstract
A first part of this review is devoted to a summary of our extensive studies of the discovery potential for instanton (I)-induced, deep-inelastic processes at HERA. Included are some key issues about I-perturbation theory, an exploitation of crucial lattice constraints and a status report about the recent I-search results by the HERA collaborations H1 and ZEUS in relation to our predictions. Next follows a brief outline of an ongoing project concerning a broad exploration of the discovery potential for hard instanton processes at the LHC. I then turn to an overview of our work on high-energy processes, involving larger-sized instantons. I shall mainly focus on the phenomenon of saturation at small Bjorken-x from an instanton perspective. In such a framework, the saturation scale is associated with the conspicuous average instanton size, $\langle\rho\rangle \sim 0.5$ fm, as known from lattice simulations. A further main result is the intriguing identification of the "Colour Glass Condensate" with the QCD *sphaleron* state.

1 Setting the stage

Instantons represent a basic non-perturbative aspect of non-abelian gauge theories like QCD. They were theoretically discovered and first studied by Belavin *et al.* [1] and 't Hooft [2], about 30 years ago.

Due to their rich vacuum structure, QCD and similar theories include topologically non-trivial fluctuations of the gauge fields, which in general carry a conserved, integer topological charge Q. Instantons ($Q = +1$) and anti-instantons ($Q = -1$) represent the simplest building blocks of topologically non-trivial vacuum structure. They are explicit solutions of the euclidean field equations in four dimensions [1]. They are known to play an important rôle in the transition region between a partonic and a hadronic description of strong interactions [3]. Yet, despite substantial theoretical evidence for the importance of instantons in chiral symmetry breaking and hadron spectroscopy, their direct experimental verification is lacking until now.

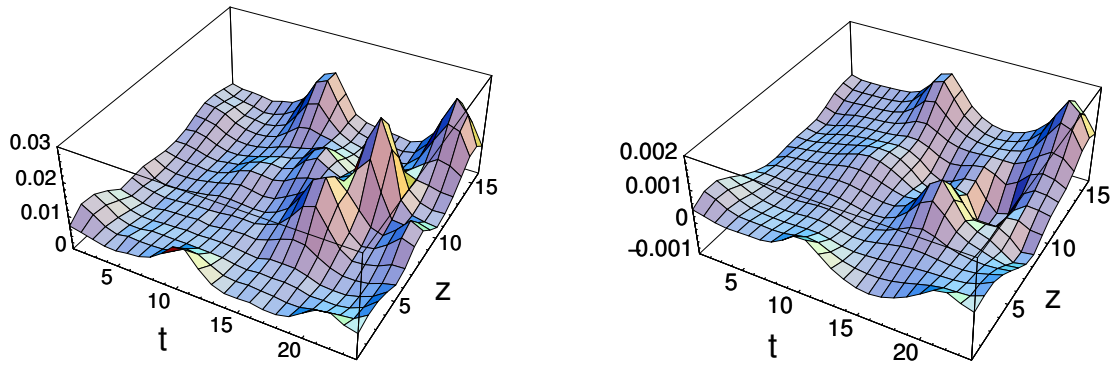

Fig. 1: Contribution from three instantons ($Q = +1$) and two anti-instantons ($Q = -1$) to the Lagrangian (left)) and the topological charge density (right) in a lattice simulation [4] (after cooling). The euclidean coordinates x and y are kept fixed while the dependence on z and t is displayed.

It turns out, however, that a characteristic *short distance* manifestation of instantons can be exploited [5] for an experimental search: Instantons induce certain (hard) processes that are forbidden in usual perturbative QCD. These involve all (light) quark flavours democratically along with a violation of chirality, in accord with the general chiral anomaly relation [2]. Based on this crucial observation, deep-inelastic scattering (DIS) at HERA has been shown to offer a unique opportunity [5] to discover such instanton-induced processes. It is of particular importance that a theoretical prediction of both the corresponding rate [6–8] and the characteristic event signature [5, 10–12] is possible in this hard scattering regime[1]. The instanton-induced cross section turns out to be in a measurable range [7, 10]. Crucial information on the region of validity for this important result, based on instanton-perturbation theory, comes from a high-quality lattice simulation [8, 13]. Another interesting possible spin-dependent signature of instantons in DIS, in form of a characteristic azimuthal spin asymmetry, has recently been discussed in Ref. [14].

In a first part (Sect. 2), I shall review our extensive investigations of deep-inelastic processes induced by small instantons. This includes a "flow-chart" of our calculations based on I-perturbation theory [6, 7], an exploitation of crucial lattice constraints [8, 13] and a confrontation [12] of the recent I-search results by the HERA collaborations H1 and ZEUS [15, 16] with our predictions. Next I shall briefly outline in Sect. 3 an ongoing project [17] to investigate theoretically and phenomenologically the discovery potential of hard instanton processes at the LHC. In Sect. 4, I then turn to an overview of our work [18–21] on high-energy processes involving larger-sized instantons. I shall focus mainly on the important theoretical challenge of the phenomenon of saturation at small Bjorken-x from an instanton perspective. In such a framework we found [18–21] that the conspicuous average instanton size scale, $\langle\rho\rangle \sim 0.5$ fm, as known from lattice simulations [13], plays the rôle of the saturation scale. As a further main and intriguing result, we were led to associate the "Colour Glass Condensate" [22] with the QCD *sphaleron* state [23]. For another more recent approach to small-x saturation in an instanton background with main emphasis on Wilson loop scattering and lacking direct lattice input, see Ref. [24]. The conclusions of this overview may be found in Sect. 5.

2 Small instantons in deep-inelastic scattering

2.1 Instanton-perturbation theory

Let us start by briefly summarizing the essence of our theoretical calculations [6, 7] based on so-called I-perturbation theory. As we shall see below, in an appropriate phase-space region of deep-inelastic scattering with generic hard scale $\mathcal{Q}$, the contributing I's and $\overline{I}$'s have *small size* $\rho \lesssim \mathcal{O}(\frac{1}{\alpha_s(\mathcal{Q})\mathcal{Q}})$ and may be self-consistently considered as a *dilute* gas, with the small QCD coupling $\alpha_s(\mathcal{Q})$ being the expansion parameter like in usual perturbative QCD (pQCD). Unlike the familiar expansion about the trivial vacuum $A_\mu^{(0)} = 0$ in pQCD, in I-perturbation theory the path integral for the generating functional of the Green's functions in Euclidean position space is then expanded about the known, classical one-instanton solution, $A_\mu = A_\mu^{(I)}(x) + \ldots$. After Fourier transformation to momentum space, LSZ amputation and careful analytic continuation to Minkowski space (where the actual on-shell limits are taken), one obtains a corresponding set of modified Feynman rules for calculating I-induced scattering amplitudes. As a further prerequisite, the masses m_q of the active quark flavours must be light on the scale of the inverse effective I-size $1/\rho_{\rm eff}$, i. e. $\mathrm{m}_q \cdot \rho_{\rm eff} \ll 1$. The leading, I-induced, chirality-violating process in the deep-inelastic regime of $e^{\pm}$P scattering is displayed in Fig. 2 (left) for $n_f = 3$ massless flavors. In the background of an I ($\overline{I}$) (of topological charge $Q = +1$ (-1)), all n_f massless quarks and anti-quarks are right (left)-handed such that the I-induced subprocess emphasized in the dotted box of Fig. 2 (left) involves a violation of chirality $Q_5 = \#\,(q_{\rm R} + \overline{q}_{\rm R}) - \#\,(q_{\rm L} + \overline{q}_{\rm L})$ by an amount,

$$\Delta Q_5 = 2\,n_f\,Q, \tag{1}$$

[1] For an exploratory calculation of the instanton contribution to the gluon-structure function, see Ref. [9].

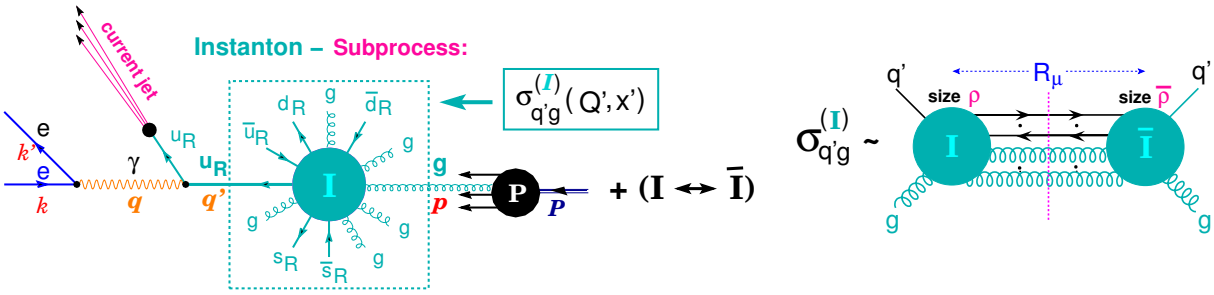

Fig. 2: (left): Leading, instanton-induced process in deep-inelastic $e^{\pm}\mathrm{P}$ scattering for $n_f = 3$ massless flavours. (right): Structure of the total cross section $\sigma^{(I)}_{q'\,g}$ for the chirality-violating "instanton-subprocess" $q'\,g \overset{(I)}{\Rightarrow} X$ according to the optical theorem. Note the illustration of the collective coordinates $\rho, \overline{\rho}$ and R_μ.

in accord with the general chiral anomaly relation [2]. Within I-perturbation theory, one first of all derives the following factorized expression in the Bjorken limit of the I-subprocess variables Q'^2 and x' (c. f. Fig. 2 (left)):

$$\frac{\mathrm{d}\sigma^{(I)}_{\mathrm{HERA}}}{\mathrm{d}x'\mathrm{d}Q'^2} \simeq \frac{\mathrm{d}\mathcal{L}^{(I)}_{q'g}}{\mathrm{d}x'\mathrm{d}Q'^2} \cdot \sigma^{(I)}_{q'g}(Q', x') \quad \text{for} \quad \left\{ \begin{array}{l} Q'^2 = -q'^2 > 0 \text{ large}, \\ 0 \leq x' = \frac{Q'^2}{2p\cdot q'} \leq 1 \text{ fixed}\,. \end{array} \right. \tag{2}$$

In Eq. (2), the differential luminosity, $\mathrm{d}\mathcal{L}^{(I)}_{q'\,g}$ counts the number of $q'\,g$ collisions per eP collisions. It is given in terms of integrals over the gluon density, the virtual photon flux, and the (known) flux of the virtual quark q' in the instanton background [7].

The essential instanton dynamics resides, however, in the total cross-section of the I-subprocess $q'\,g \overset{I}{\Rightarrow} X$ (dotted box of Fig. 2 (left) and Fig. 2 (right)). Being an observable, $\sigma^{(I)}_{q'g}(Q', x')$ involves integrations over all I and $\overline{I}$-"collective coordinates", i. e. the I ($\overline{I}$) sizes ρ ($\overline{\rho}$), the $I\overline{I}$ distance four-vector R_μ and the relative $I\overline{I}$ color orientation matrix U.

$$\sigma^{(I)}_{q'\,g} = \int d^4R\, \mathrm{e}^{\mathrm{i}\,(p+q')\cdot R} \int_0^\infty d\rho \int_0^\infty d\overline{\rho}\, \mathrm{e}^{-(\rho+\overline{\rho})Q'}\; D(\rho)\, D(\overline{\rho}\,) \int dU\, \mathrm{e}^{-\frac{4\pi}{\alpha_s}\,\Omega\left(U, \frac{R^2}{\rho\overline{\rho}}, \frac{\overline{\rho}}{\rho}\right)} \{\ldots\} \tag{3}$$

Both instanton and anti-instanton degrees of freedom enter here, since the I-induced cross-section results from taking the modulus squared of an amplitude in the single I-background. Alternatively and more conveniently (c. f. Fig. 2 (right)), one may invoke the optical theorem to obtain the cross-section (3) in Minkowski space as a discontinuity of the $q'\,g$ forward elastic scattering amplitude in the $I\overline{I}$-background [7]. The $\{\ldots\}$ in Eq. (3) abreviates smooth contributions associated with the external partons etc. Let us concentrate on two crucial and strongly varying quantities of the I-calculus appearing in Eq. (3): $D(\rho)$, the (reduced) I-size distribution [2, 28], and $\Omega\left(U, \frac{R^2}{\rho\overline{\rho}}, \frac{\overline{\rho}}{\rho}\right)$, the $I\overline{I}$ interaction, associated with a resummation of final-state gluons. Both objects are *known* within I-perturbation theory, formally for $\alpha_s(\mu_r)\ln(\mu_r\,\rho) \ll 1$ and $\frac{R^2}{\rho\overline{\rho}} \gg 1$ (diluteness), respectively, with μ_r being the renormalization scale. In the $I\overline{I}$-valley approach [25], the functional form of $\Omega^{I\bar{I}}_{\mathrm{valley}}$ is analytically known [26, 27] (formally) for *all* values of $R^2/(\rho\bar{\rho})$. The *actual* region of validity of the valley approach is an important issue to be addressed again later.

Most importantly, the resulting power-law behaviour for the I-size distribution,

$$D(\rho) \propto \rho^{\beta_0 - 5 + \mathcal{O}(\alpha_s)}, \tag{4}$$

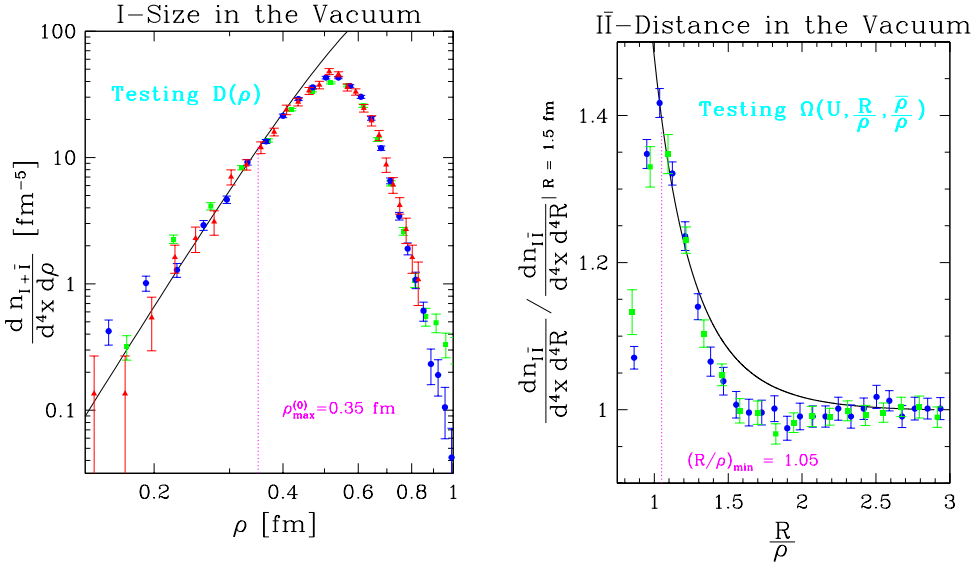

Fig. 3: Illustration of the agreement of recent high-quality lattice data [8,13] for the instanton-size distribution (left) and the normalized $I\overline{I}$-distance distribution (right) with the predictions from instanton-perturbation theory [8] for $\rho \lesssim 0.35$ fm and $R/\rho \gtrsim 1.05$, respectively. $\alpha^{3-\text{loop}}_{\overline{\text{MS}}}$ with $\Lambda^{(n_f=0)}_{\overline{\text{MS}}}$ from the ALPHA collaboration [29] was used.

involving the leading QCD β-function coefficient, $\beta_0 = \frac{11}{3}\,N_c - \frac{2}{3}\,n_f$, $(N_c = 3)$, generically spoils the calculability of I-observables due to the bad IR-divergence of the integrations over the I $(\overline{I}\,)$-sizes for large ρ $(\overline{\rho}\,)$. Deep-inelastic scattering represents, however, a crucial exception: The *exponential* "form factor" $\exp(-Q'(\rho+\overline{\rho}\,))$ that was shown [6] to arise in Eq. (3), insures convergence and *small* instantons for large enough Q', despite the strong power-law growth of $D(\rho)$. This is the key feature, warranting the calculability of I-predictions for DIS.

It turns out that for (large) $Q' \neq 0$, all collective coordinate integrations in $\sigma^{(I)}_{q'g}$ of Eq. (3) may be performed in terms of a *unique saddle point*:

$$\begin{aligned} U^* \quad &\Leftrightarrow \quad \text{most attractive relative } I\overline{I} \text{ orientation in color space,} \\ \rho^* \quad &= \quad \overline{\rho}^* \sim \frac{4\pi}{\alpha_s(\frac{1}{\rho^*})}\,\frac{1}{Q'}; \quad \frac{R^{*\,2}}{\rho^{*\,2}} \overset{Q'\ \text{large}}{\sim} 4\frac{x'}{1-x'} \end{aligned} \tag{5}$$

This result underligns the self-consistency of the approach, since for large Q' and small $(1-x')$ the saddle point (5), indeed, corresponds to widely separated, small I's and $\overline{I}$'s.

2.2 Crucial impact of lattice results

The I-size distribution $D(\rho)$ and the $I\overline{I}$ interaction $\Omega\left(U, \frac{R^2}{\rho\overline{\rho}}, \frac{\overline{\rho}}{\rho}\right)$ form a crucial link between deep-inelastic scattering and lattice observables in the QCD vacuum [8].

Lattice simulations, on the other hand, provide independent, non-perturbative information on the *actual* range of validity of the form predicted from I-perturbation theory for these important functions of ρ and R/ρ, respectively. The one-to-one saddle-point correspondence (5) of the (effective) collective I-coordinates $(\rho^*, R^*/\rho^*)$ to (Q', x') may then be exploited to arrive at a "fiducial" (Q', x') region for our predictions in DIS. Let us briefly summarize the results of this strategy [8].

We have used the high-quality lattice data [8, 13] for quenched QCD $(n_f = 0)$ by the UKQCD collaboration together with the careful, non-perturbative lattice determination of the respective QCD Λ-parameter, $\Lambda^{(n_f=0)}_{\overline{\text{MS}}} = (238 \pm 19)$ MeV, by the ALPHA collaboration [29]. The results of an essentially parameter-free comparison of the continuum limit [8] for the simulated $(I + \overline{I}\,)$-size and the

$I\overline{I}$-distance distributions with I-perturbation theory versus ρ and R/ρ, respectively, is displayed in Fig. 3. The UKQCD data for the $I\overline{I}$-distance distribution provide the first direct test of the $I\overline{I}$ interaction $\Omega\left(U, \frac{R^2}{\rho\overline{\rho}}, \frac{\overline{\rho}}{\rho}\right)$ from the $I\overline{I}$-valley approach via [8]

$$\frac{\mathrm{d}\, n_{I\overline{I}}}{\mathrm{d}^4x\, \mathrm{d}^4R}_{|\mathrm{UKQCD}} \stackrel{?}{\simeq} \int_0^\infty d\rho \int_0^\infty d\overline{\rho}\, D(\rho)\, D(\overline{\rho}) \int dU\, \mathrm{e}^{-\frac{4\pi}{\alpha_s}\Omega\left(U, \frac{R^2}{\rho\overline{\rho}}, \frac{\overline{\rho}}{\rho}\right)}, \tag{6}$$

and the lattice measurements of $D(\rho)$.

From Fig. 3, I-perturbation theory appears to be quantitatively valid for

$$\left.\begin{array}{lcl} \rho \cdot \Lambda_{\overline{\mathrm{MS}}}^{(n_f=0)} & \lesssim & 0.42 \\ R/\rho & \gtrsim & 1.05 \end{array}\right\} \stackrel{\textbf{saddle point}}{\Rightarrow} \left\{\begin{array}{lcl} Q'/\Lambda_{\overline{\mathrm{MS}}}^{(n_f)} & \gtrsim & 30.8, \\ x' & \gtrsim & 0.35, \end{array}\right. \tag{7}$$

Beyond providing a quantitative estimate for the "fiducial" momentum space region in DIS, the good, parameter-free agreement of the lattice data with I-perturbation theory is very interesting in its own right. Uncertainties associated with the inequalities (7) are studied in detail in Ref. [12].

2.3 Characteristic final-state signature

The qualitative origin of the characteristic final-state signature of I-induced events is intuitively explained and illustrated in Fig. 4. An indispensable tool for a quantitative investigation of the characteristic final-state signature and notably for actual experimental searches of I-induced events at HERA is our Monte-Carlo generator package QCDINS [10].

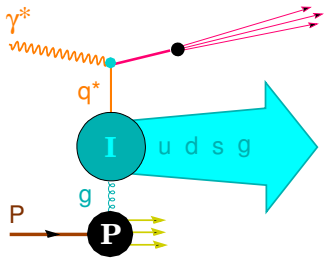

current **jet**

"band"-region: "Fireball" decaying *isotropically* (in I-rest system) into $n_f\,(q+\overline{q}) + \mathcal{O}(\frac{1}{\alpha_s})\, g = \mathcal{O}(10)$ partons

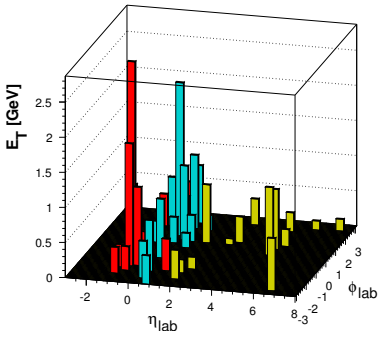

Fig. 4: Characteristic signature of I-induced events: *One* (current) *jet* along with a densely filled *band* of hadrons in the (η, ϕ) plane. Each event has large hadron multiplicity, large total E_t, u-d-s flavor democracy with 1 $s\overline{s}$-pair/event leading to $K's, \Lambda's \ldots$. An event from our QCDINS [10] generator (right) illustrates these features.

2.4 Status of searches at HERA

The results of dedicated searches for instanton-induced events by the H1 and ZEUS collaborations [15, 16], based on our theoretical work, have been finalized meanwhile. The H1 analysis was based on $\int \mathcal{L}dt \approx 21$ pb^{-1}, while ZEUS used $\int \mathcal{L}dt \approx 38$ pb^{-1}, with somewhat differing kinematical cuts. Since the upgraded HERA II machine is now performing very well, forthcoming searches based on a several times higher luminosity might turn out most interesting. Let me briefly summarize the present status from a theorist's perspective.

While H1 indeed observed a statistically significant excess of events with instanton-like topology and in good agreement with the theoretical predictions, *physical* significance could not be claimed, due to remaining uncertainties in the standard DIS (sDIS) background simulation. The ZEUS collaboration

Table 1: Comparison of implemented fiducial cuts that are required in principle to warrant the validity of I-perturbation theory.

Fiducial	Cuts		**H1**	**ZEUS**
Q^2	$\gtrsim$	113 GeV^2 ?	**no**	**yes**
Q'^2	$\gtrsim$	113 GeV^2 ?	**yes**	**yes**
x'	$\gtrsim$	0.35 ?	**no**	**no**

obtained a conservative, background-independent upper limit on the instanton-induced HERA cross section of 26 pb@95% CL, to be compared to our theoretical prediction of 8.9 pb for the given cuts. In both experiments it was demonstrated that a decisive experimental test of the theoretical predictions based on I-perturbation theory is well within reach in the near-future. In view of the present situation and the interesting prospects for HERA II, let me proceed with a number of comments.

A first important task consists in reconstructing the instanton-subprocess variables (Q'^2, x') from Eq. (2) and in implementing the theoretically required fiducial cuts (cf. Eq. (7)). The actual status is displayed in Table 1 for comparison. The implications of the lacking x'-cut both in the H1 and ZEUS data are presumably not too serious, since QCDINS — *with* its default x'-cut — models to some extent the sharp suppression of I-effects, apparent in the lattice data (cf. Fig. 3 (right)) for $R/\rho \lesssim 1.0 - 1.05$, i.e. $x' \lesssim 0.3 - 0.35$. Yet, this lacking, experimental cut introduces a substantial uncertainty in the predicted magnitude of the I-signal that hopefully may be eliminated soon. The lacking Q^2-cut in the H1 data is potentially more serious. As a brief reminder [6, 10], this cut assures in particular the dominance of "planar" handbag-type graphs in $\sigma^{(I)}_{\rm HERA}$ and all final-state observables. Because of computational complications, the non-planar contributions are *not* implemented in the QCDINS event generator, corresponding to unreliable QCDINS results for small Q^2.

The main remaining challenge resides in the fairly large sDIS background uncertainties. The essential reason is that the existing Monte Carlo generators have been typically designed and tested for kinematical regions different from where the instanton signal is expected! Although the residual problematics is not primarily related to lacking statistics, the near-future availability of many more events will allow to strengthen the cuts and thus hopefully to increase the gap between signal and background. A common search strategy consists in producing I-enriched data samples by cutting on several discriminating observables, each one being sensitive to *different* basic instanton characteristics. An optimized set may be found according to the highest possible

$$\text{instanton separation power} = \frac{\epsilon_I}{\epsilon_{\rm sDIS}}, \tag{8}$$

in terms of the sDIS and instanton efficiencies, with $\epsilon_I \gtrsim 5 - 10\%$. Substantial enhancements of the instanton sensitivity were obtained, by means of various multivariate discrimination methods, involving only a single cut on a suitable discriminant variable. In case of ZEUS, cuts on the Fisher discriminant have been used to obtain instanton-enhanced subsamples.

Let me summarize the results obtained so far in form of a theorist's "unified plot" of the H1 and ZEUS "excess" versus the I-separation power. Any visible correlation of a rising *experimental* "excess" with the (Monte-Carlo) *theoretical* I-separation power in Fig. 5 would be an intriguing first signature for a signal. The behaviour seen from the end of the ZEUS range into the H1 domain, might indeed suggest some increase of the excess towards rising I-sparation power. The comparatively low I-separation power of the ZEUS data (and thus perhaps also their *negative* excess?) is mainly due to the implementation of the fiducial cut in Q^2 that is lacking in case of H1.

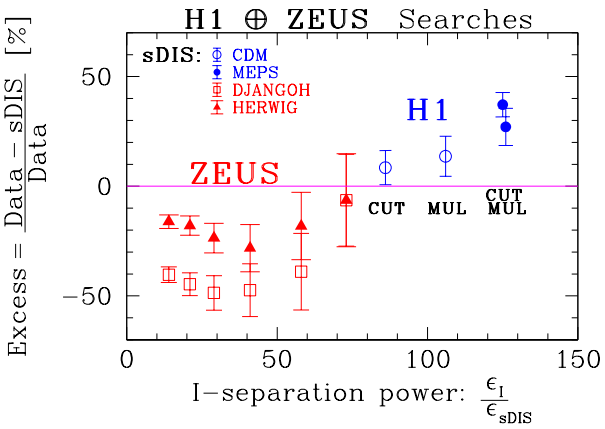

Fig. 5: A theorist's "unified plot" of the H1 and ZEUS "excess" versus I-separation power. The H1 and ZEUS data are seen to join smoothly. A first sign of a rising excess towards higher separation powers might be suspected.

3 Study of the discovery potential at the LHC

Given our extended experience with instanton physics both theoretically and experimentally at DESY, it is natural to ask about the discovery potential for instanton-induced processes at the forthcoming LHC. Indeed, a respective project has been set up around a theoretical PhD Thesis [17], but is still in a relatively early stage.

3.1 Outline of the project

We attempt to do a broad study, focussing both on theoretical and phenomenological issues. Let me just enumerate some interesting aspects that differ essentially from the familiar situation for spacelike hard scattering in DIS at HERA.

Theoretically: The first and foremost task is to identify and calculate the leading I-subprocess at the LHC within I-perturbation theory. Unlike HERA (Fig. 2 (left)), one starts from a $g\,g$-initial state at the LHC. Hence, the rate will be enhanced by a factor $\propto \frac{1}{\alpha_{\rm e.m.}\,\alpha_s}$ compared to $\gamma^*\,g$ scattering at HERA. Then, the next crucial question is how to enforce some parton virtuality in the respective instanton-induced $g\,g$-subprocess, such as to retain the applicability of I-perturbation theory.

An interesting possibility we are exploring is to enter the required virtuality through the *final state* in case of the LHC! One may consider the fragmentation of one or even two outgoing quarks from the $g\,g$-initiated I-instanton subprocess into a *large* $E_\perp$ photon or W-boson and other particles. The requirement of large $E_\perp$ then enforces a *timelike* virtuality onto the outgoing parent quark.

Experimentally: Crucial criteria will be a good signature paired with the lowest possible background, as well as a good trigger. At the experimental front we forsee the collaboration of T. Carli/CERN, who will be able to merge his actual knowledge of the LHC with many years of experience from searches for instantons at HERA. After the theoretical calculations are under control, the next task is to adapt our QCDINS event generator to the LHC, to work out characteristic event signatures, optimal observables, fiducial cuts etc.

4 Instanton-driven saturation at small x

One of the most important observations from HERA is the strong rise of the gluon distribution at small Bjorken-x [30]. On the one hand, this rise is predicted by the DGLAP evolution equations [31] at high Q^2 and thus supports QCD [32]. On the other hand, an undamped rise will eventually violate unitarity. The reason for the latter problem is known to be buried in the linear nature of the DGLAP- and the BFKL-equations [33]: For decreasing Bjorken-x, the number of partons in the proton rises, while their

effective size $\sim 1/Q$ increases with decreasing Q^2. At some characteristic scale $Q^2 \approx Q_s^2(x)$, the gluons in the proton start to overlap and so the linear approximation is no longer applicable; non-linear corrections to the linear evolution equations [34] arise and become significant, potentially taming the growth of the gluon distribution towards a "saturating" behaviour.

From a theoretical perspective, eP-scattering at small Bjorken-x and decreasing Q^2 uncovers a novel regime of QCD, where the coupling α_s is (still) small, but the parton densities are so large that conventional perturbation theory ceases to be applicable, eventually. Much interest has recently been generated through association of the saturation phenomenon with a multiparticle quantum state of high occupation numbers, the "Colour Glass Condensate" that correspondingly, can be viewed [22] as a strong *classical* colour field $\propto 1/\sqrt{\alpha_s}$.

4.1 Why instantons?

Being extended non-perturbative fluctuations of the gluon field, instantons come to mind naturally in the context of saturation, since

- classical *non-perturbative* colour fields are physically appropriate in this regime; I-interactions always involve many non-perturbative gluons with multiplicity $\langle n_g \rangle \propto \frac{1}{\alpha_s}$!
- the functional form of the instanton gauge field is explicitely known and its strength is $A_\mu^{(I)} \propto \frac{1}{\sqrt{\alpha_s}}$ as needed;
- an identification of the "Colour Glass Condensate" with the QCD-sphaleron state appears very suggestive [20, 21] (cf. below and Sec 4.4).
- At high energies ($x \to 0$), larger I-sizes ($\rho \gtrsim 0.35$ fm) are probed! Unlike DIS, now the sharply defined average I-size $\langle \rho \rangle \approx 0.5$ fm (known from lattice simulations [13]) comes into play and becomes a relevant and conspicuous length scale in this regime (cf. Fig. 6 (left)).
- An intriguing observation is that the I-size scale $\langle \rho \rangle$ coincides surprisingly well with the transverse resolution $\Delta x_\perp \sim 1/Q$, where the small-x rise of the structure function $F_2(x, Q^2)$ *abruptly* starts to *increase* with falling $\Delta x_\perp$! This striking feature[2] is illustrated in Fig. 6 (right), with the power $\lambda(Q)$ being defined via the ansatz $F_2(x, Q^2) = c(Q)\, x^{-\lambda(Q)}$ at small x. A suggestive interpretation is that instantons are getting resolved for $\Delta x_\perp \lesssim \langle \rho \rangle$.
- We know already from I-perturbation theory that the instanton contribution tends to strongly increase towards the softer regime [5,7,10]. The mechanism for the decreasing instanton suppression with increasing energy is known since a long time [35,36]: Feeding increasing energy into the scattering process makes the picture shift from one of tunneling between adjacent vacua ($E \approx 0$) to that of the actual creation of the sphaleron-like, coherent multi-gluon configuration [23] on top of the potential barrier of height [5, 37] $E = m_{\rm sph} \propto \frac{1}{\alpha_s \rho_{\rm eff.}}$.

4.2 From instanton-perturbation theory to saturation

The investigation of saturation becomes most transparent in the familiar colour-dipole picture [38] (cf. Fig. 7 (left)), notably if analyzed in the so-called dipole frame [39]. In this frame, most of the energy is still carried by the hadron, but the virtual photon is sufficiently energetic, to dissociate before scattering into a $q\bar{q}$-pair (a *colour dipole*), which then scatters off the hadron. Since the latter is Lorentz-contracted, the dipole sees it as a colour source of transverse extent, living (essentially) on the light cone. This colour field is created by the constituents of the well developed hadron wave function and – in view of its high intensity, i.e. large occupation numbers – can be considered as classical. Its strength near saturation is $\mathcal{O}(1/\sqrt{\alpha_s})$. At high energies, the lifetime of the $q\overline{q}$-dipole is much larger than the interaction time

[2] I wish to thank A. Levy for the experimental data in Fig. 6 (right)

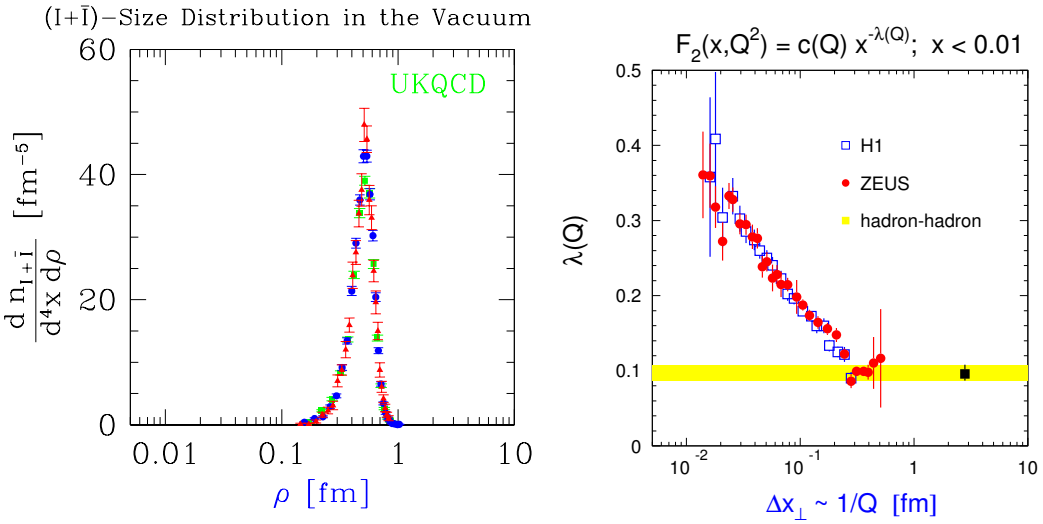

Fig. 6: The I-size scale $\langle\rho\rangle$ from lattice data [8,13] (left) coincides surprisingly well with the transverse resolution $\Delta x_\perp \sim 1/Q$, where the small-x rise of the structure function $F_2(x,Q^2)$ *abruptly* starts to *increase* with falling $\Delta x_\perp$ (right).

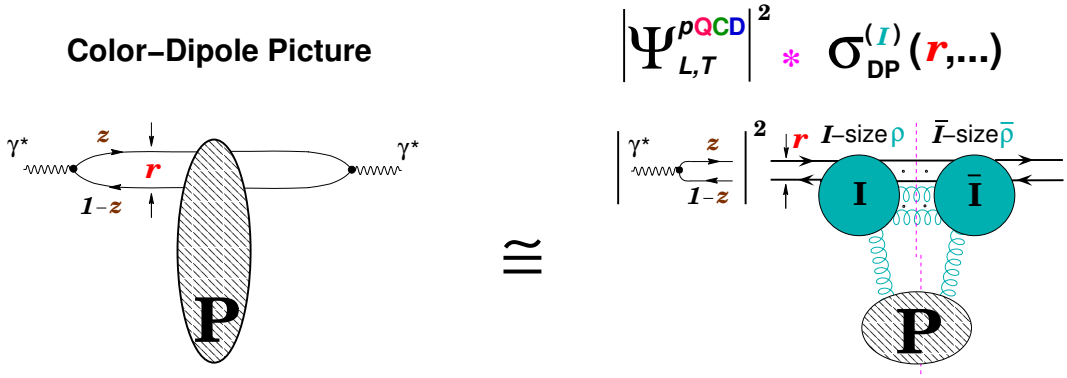

Fig. 7: Illustration of the color dipole picture, its associated variables, the factorization property and the structure of the dipole cross section in an instanton approach.

between this $q\overline{q}$-pair and the hadron and hence, at small $x_{\rm Bj}$, this gives rise to the familiar factorized expression of the inclusive photon-proton cross sections,

$$\sigma_{L,T}(x_{\rm Bj},Q^2) = \int_0^1 dz \int d^2\,r\;|\Psi_{L,T}(z,r)|^2\,\sigma_{\rm DP}(r,\ldots). \tag{9}$$

Here, $|\Psi_{L,T}(z,r)|^2$ denotes the modulus squared of the (light-cone) wave function of the virtual photon, calculable in pQCD, and $\sigma_{\rm DP}(r,\ldots)$ is the $q\overline{q}$-dipole - nucleon cross section. The variables in Eq. (9) are the transverse $(q\overline{q})$-size $\mathbf{r}$ and the photon's longitudinal momentum fraction z carried by the quark. The dipole cross section is expected to include in general the main non-perturbative contributions. For small r, one finds within pQCD [38, 40] that $\sigma_{\rm DP}$ vanishes with the area πr^2 of the $q\overline{q}$-dipole. Besides this phenomenon of "colour transparency" for small $r = |r|$, the dipole cross section is expected to saturate towards a constant, once the $q\overline{q}$-separation r exceeds a certain saturation scale r_s (cf. Fig. 7 (right)). While there is no direct proof of the saturation phenomenon, successful models incorporating saturation do exist [41] and describe the data efficiently.

Let us outline more precisely our underlying strategy:

– We start from the large Q^2 regime and appropriate cuts such that I-perturbation theory is strictly

valid. The corresponding, known results on I-induced DIS processes [6] are then transformed into the colour-dipole picture.

– The guiding question is: Can background instantons of size $\sim \langle\rho\rangle$ give rise to a saturating, geometrical form for the dipole cross section,

$$\sigma_{\rm DP}^{(I)}(r,\ldots) \overset{r \gtrsim \langle\rho\rangle}{\sim} \pi\langle\rho\rangle^2. \tag{10}$$

– With the crucial help of lattice results, the $q\bar{q}$-dipole size r is next carefully increased towards hadronic dimensions. Thanks to the lattice input, IR divergencies are removed and the original cuts are no longer necessary.

4.3 The simplest process: $\gamma^* + g \overset{(I)}{\to} q_{\rm R} + \overline{q}_{\rm R}$

Let us briefly consider first the simplest I-induced process, $\gamma^*\, g \Rightarrow q_{\rm R}\overline{q}_{\rm R}$, with one flavour and no final-state gluons. More details may be found in Ref. [20]. Already this simplest case illustrates transparently that in the presence of a background instanton, the dipole cross section indeed saturates with a saturation scale of the order of the average I-size $\langle\rho\rangle$.

We start by recalling the results for the total $\gamma^* N$ cross section within I-perturbation theory from Ref. [6],

$$\sigma_{L,T}(x_{\rm Bj},Q^2) \;=\; \int\limits_{x_{\rm Bj}}^{1} \frac{dx}{x}\left(\frac{x_{\rm Bj}}{x}\right) G\left(\frac{x_{\rm Bj}}{x},\mu^2\right) \int dt \frac{d\hat{\sigma}_{L,T}^{\gamma^* g}(x,t,Q^2)}{dt}; \tag{11}$$

$$\frac{d\hat{\sigma}_{L}^{\gamma^* g}}{dt} \;=\; \frac{\pi^7}{2}\frac{e_q^2}{Q^2}\frac{\alpha_{\rm em}}{\alpha_{\rm s}}\left[x(1-x)\sqrt{tu}\,\frac{\mathcal{R}(\sqrt{-t})-\mathcal{R}(Q)}{t+Q^2} - (t\leftrightarrow u)\right]^2, \tag{12}$$

with a similar expression for $d\hat{\sigma}_T^{\gamma^*\, g}/d\,t$. Here, $G\left(x_{\rm Bj},\mu^2\right)$ denotes the gluon density and L,T refers to longitudinal and transverse photons, respectively.

Note that Eqs. (11), (12) involve the resolution dependent length scale

$$\mathcal{R}(\mathcal{Q}) = \int_0^\infty d\rho\; D(\rho)\rho^5(\mathcal{Q}\rho){\rm K}_1(\mathcal{Q}\rho). \tag{13}$$

which is of key importance for continuing towards $\mathcal{Q}\langle\rho\rangle \Rightarrow 0$! For sufficiently large $\mathcal{Q}\langle\rho\rangle$, the crucial factor $(\mathcal{Q}\rho)\,K_1(\mathcal{Q}\rho) \sim e^{-\mathcal{Q}\rho}$ in Eq.(13) exponentially suppresses large size instantons and I-perturbation theory holds, as shown first in Ref. [6]. In our continuation task towards smaller $\mathcal{Q}\langle\rho\rangle$, crucial lattice information enters. We recall that the I-size distribution $D_{\rm lattice}(\rho)$, as *measured* on the lattice [8, 12, 13], is strongly peaked around an average I-size $\langle\rho\rangle \approx 0.5$ fm, while being in excellent agreement with I-perturbation theory for $\rho \lesssim 0.35$ fm (cf. Sect. 2.2 and Fig. 3(left)). Our strategy is thus to generally identify $D(\rho) = D_{\rm lattice}(\rho)$ in Eq.(13), whence

$$\mathcal{R}(0) = \int_0^\infty d\rho\; D_{\rm lattice}(\rho)\rho^5 \approx 0.3 \text{ fm} \tag{14}$$

becomes finite and a $\mathcal{Q}^2$ cut is no longer necessary.

By means of an appropriate change of variables and a subsequent $2d$-Fourier transformation, Eqs. (11), (12) may indeed be cast [20] into a colour-dipole form (9), e.g. (with $\hat{Q} = \sqrt{z\,(1-z)}\,Q$)

$$\left(|\Psi_L|^2\,\sigma_{\rm DP}\right)^{(I)} \approx |\;\Psi_L^{\rm pQCD}(z,r)\;|^2\;\frac{1}{\alpha_{\rm s}}\,x_{\rm Bj}\,G(x_{\rm Bj},\mu^2)\,\frac{\pi^8}{12} \tag{15}$$

$$\times \left\{ \int_0^\infty d\rho D(\rho)\, \rho^5 \left(\frac{-\frac{d}{dr^2}\left(2r^2 \frac{\mathrm{K}_1(\hat{Q}\sqrt{r^2+\rho^2/z})}{\hat{Q}\sqrt{r^2+\rho^2/z}} \right)}{\mathrm{K}_0(\hat{Q}r)} - (z \leftrightarrow 1-z) \right) \right\}^2 .$$

The strong peaking of $D_{\mathrm{lattice}}(\rho)$ around $\rho \approx \langle\rho\rangle$, implies

$$\left(|\Psi_{L,T}|^2 \sigma_{\mathrm{DP}}\right)^{(I)} \Rightarrow \begin{cases} \mathcal{O}(1) \text{ but exponentially small}; & r \to 0, \\ \mid \Psi_{L,T}^{\mathrm{pQCD}} \mid^2 \frac{1}{\alpha_{\mathrm{s}}}\, x_{\mathrm{Bj}}\, G(x_{\mathrm{Bj}}, \mu^2)\, \frac{\pi^8}{12}\, \mathcal{R}(0)^2; & \frac{r}{\langle\rho\rangle} \gtrsim 1. \end{cases} \tag{16}$$

Hence, the association of the intrinsic instanton scale $\langle\rho\rangle$ with the saturation scale r_s becomes apparent from Eqs. (15), (16): $\sigma_{\mathrm{DP}}^{(I)}(r, \ldots)$ rises strongly as function of r around $r_s \approx \langle\rho\rangle$, and indeed *saturates* for $r/\langle\rho\rangle > 1$ towards a *constant geometrical limit*, proportional to the area $\pi\, \mathcal{R}(0)^2 = \pi \left(\int_0^\infty d\rho\, D_{\mathrm{lattice}}(\rho)\, \rho^5 \right)^2$, subtended by the instanton. Since $\mathcal{R}(0)$ is divergent within I-perturbation theory, the information about $D(\rho)$ from the lattice (Fig. 6 (left)) is crucial for the finiteness of the result.

4.4 Identification of the color glass condensate with the QCD-sphaleron state

Next, let us consider the realistic process, $\gamma^* + g \overset{(I)}{\to} n_f\, (q_{\mathrm{R}} + \overline{q}_{\mathrm{R}}) +$ gluons. On the one hand, the inclusion of final-state gluons and $n_f > 1$ causes a significant complication. On the other hand, it is due to the effect of those gluons that the identification of the QCD-sphaleron state with the colour glass condensate has emerged [20, 21], while the qualitative "saturation" features remain unchanged. Most of the I-dynamics resides in the I-induced $q^*\, g$-subprocess with an incoming off-mass-shell quark q^* originating from photon dissociation. The important kinematical variables are the I-subprocess energy $E = \sqrt{(q'+p)^2}$ and the quark virtuality $Q'^2 = -q'^2$, with the gluon 4-momentum denoted by p_μ.

It is most convenient to account for the final-state gluons by means of the $I\bar{I}$-valley method [25] (cf. also Sect. 2.1). It allows to achieve via the optical theorem, an elegant summation over the gluons. The result leads to an exponentiation of the final-state gluon effects, residing entirely in the $I\bar{I}$-valley interaction $-1 \leq \Omega_{\mathrm{valley}}^{I\bar{I}}(\frac{R^2}{\rho\bar{\rho}} + \frac{\rho}{\bar{\rho}} + \frac{\bar{\rho}}{\rho}; U) \leq 0$, introduced in Eq. (3) of Sect. 2.1. Due to the new gluon degrees of freedom, the additional integrations over the $I\bar{I}$-distance R_μ appear (cf. Fig. 2 (right)), while the matrix U characterizes the relative $I\bar{I}$ orientation in colour space. We remember from Sect. 2.1 that the functional form of $\Omega_{\mathrm{valley}}^{I\bar{I}}$ is analytically known [26, 27] (formally) for *all* values of $R^2/(\rho\bar{\rho})$. Our strategy here is identical to the one for the "simplest process" above: Starting point is the $\gamma^* N$ cross section, this time obtained by means of the $I\bar{I}$-valley method [7]. The next step is a variable and Fourier transformation into the colour-dipole picture. The dipole cross section $\tilde{\sigma}_{\mathrm{DP}}^{(I),\mathrm{gluons}}(\mathbf{l}^2, x_{\mathrm{Bj}}, \ldots)$ before the final 2d-Fourier transformation of the quark transverse momentum $\mathbf{l}$ to the conjugate dipole size $\mathbf{r}$, arises simply as an energy integral over the I-induced total $q^* g$ cross section in Eq. (3) from Ref. [7],

$$\tilde{\sigma}_{\mathrm{DP}}^{(I),\mathrm{gluons}} \approx \frac{x_{\mathrm{Bj}}}{2}\, G(x_{\mathrm{Bj}}, \mu^2) \int_0^{E_{\max}} \frac{d\,E}{E} \left[\frac{E^4}{(E^2 + Q'^2)\, Q'^2}\, \sigma_{q^* g}^{(I)}\left(E, \mathbf{l}^2, \ldots\right) \right], \tag{17}$$

involving in turn integrations over the $I\bar{I}$-collective coordinates $\rho, \bar{\rho}, U$ and R_μ.

In the softer regime of interest for saturation, we again substitute $D(\rho) = D_{\mathrm{lattice}}(\rho)$, which enforces $\rho \approx \bar{\rho} \approx \langle\rho\rangle$ in the respective $\rho, \bar{\rho}$-integrals, while the integral over the $I\bar{I}$-distance R is dominated by a *saddle point*,

$$\frac{R}{\langle\rho\rangle} \approx \text{function}\left(\frac{E}{m_{\mathrm{sph}}}\right); \quad m_{\mathrm{sph}} \approx \frac{3\pi}{4} \frac{1}{\alpha_{\mathrm{s}}\, \langle\rho\rangle} = \mathcal{O}(\text{ few GeV }). \tag{18}$$

At this point, the mass m_{sph} of the QCD-sphaleron [5, 37], i.e the barrier height separating neighbouring topologically inequivalent vacua, enters as the scale for the energy E. The saddle-point dominance

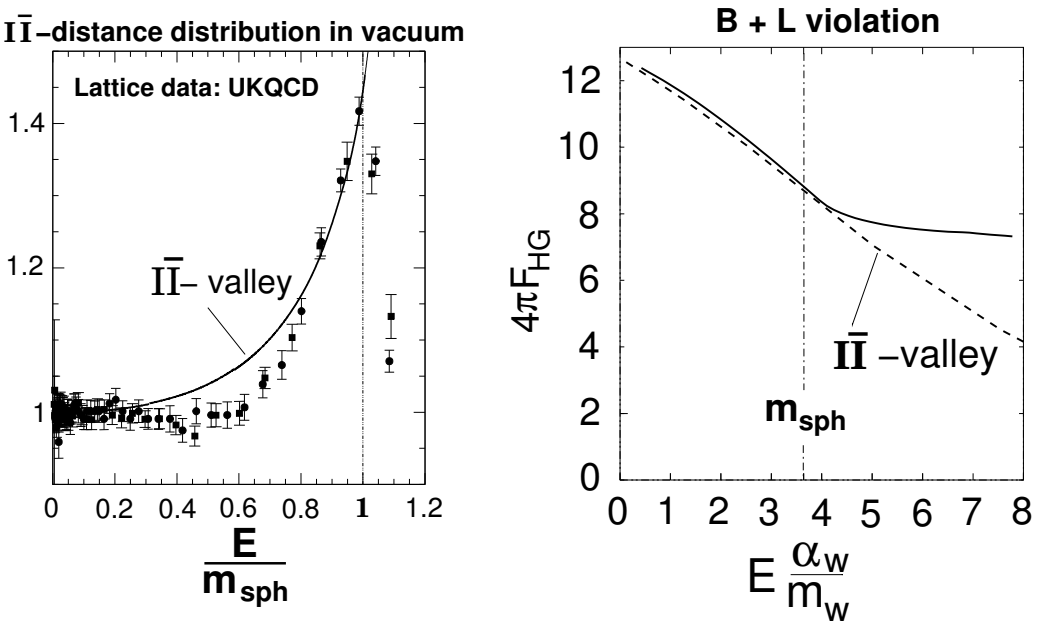

Fig. 8: (left) The UKQCD lattice data [8, 13] of the (normalized) $I\bar{I}$-distance distribution together with the corresponding $I\bar{I}$-valley prediction [20] from Fig. 3 (right) are re-displayed versus energy in units of the QCD sphaleron mass $m_{\rm sph}$.This illustrates the validity of the valley approach right until the sphaleron peak! (right) The same trend for electroweak $B+L$ -violation is apparent from an independent numerical simulation of the suppression exponent for two-particle collisions ('Holy Grail' function) $F_{\rm HG}(E)$ [42, 43]

implies a one-to-one relation,

$$\frac{R}{\langle\rho\rangle} \Leftrightarrow \frac{E}{m_{\rm sph}}; \quad \text{with } R = \langle\rho\rangle \Leftrightarrow E \approx m_{\rm sph}. \tag{19}$$

Our continuation to the saturation regime now involves crucial lattice information about $\Omega^{I\bar{I}}$. The relevant lattice observable is the distribution of the $I\bar{I}$-distance [8, 20] R, providing information on $\left\langle \exp[-\frac{4\pi}{\alpha_{\rm s}}\Omega^{I\bar{I}}]\right\rangle_{U,\rho,\bar{\rho}}$ in euclidean space (cf. Fig. 3 (right)). Due to the crucial saddle-point relation Eqs. (18, 19), we may replace the original variable $R/\langle\rho\rangle$ by $E/m_{\rm sph}$. A comparison of the respective $I\bar{I}$-valley predictions with the UKQCD lattice data [8, 13, 20] versus $E/m_{\rm sph}$ is displayed in Fig. 8 (left). It reveals the important result that the $I\bar{I}$-valley approximation is quite reliable up to $E \approx m_{\rm sph}$. Beyond this point a marked disagreement rapidly develops: While the lattice data show a *sharp peak* at $E \approx m_{\rm sph}$, the valley prediction continues to rise indefinitely for $E \gtrsim m_{\rm sph}$! It is remarkable that an extensive recent and completely independent semiclassical numerical simulation [42] shows precisely the same trend for electroweak $B + L$-violation, as displayed in Fig. 8 (right).

It is again at hand to identify $\Omega^{I\bar{I}} = \Omega^{I\bar{I}}_{\rm lattice}$ for $E \gtrsim m_{\rm sph}$. Then the integral over the I-subprocess energy spectrum (17) in the dipole cross section appears to be dominated by the sphaleron configuration at $E \approx m_{\rm sph}$. The feature of saturation analogously to the "simplest process" in Sect. 4.3 then implies the announced identification of the colour glass condensate with the QCD-sphaleron state.

5 Conclusions

As non-perturbative, topological fluctuations of the gluon fields, *instantons* are a basic aspect of QCD. Hence their experimental discovery through hard instanton-induced processes would be of fundamental significance. A first purpose of this overview was to present a summary of our systematic theoretical

and phenomenological investigations of the discovery potential in DIS at HERA, based on a calculable rate of measurable range and a characteristic "fireball"-like event signature. In a summary of the present status of experimental searches by H1 and ZEUS, the typical remaining challenges were particularly emphasized. In view of the good performance of the upgraded HERA II machine, one may expect further possibly decisive instanton search results in the near future.The existing H1 and ZEUS results have demonstrated already that the required sensitivity according to our theoretical predictions is within reach. Looking ahead, I have briefly discussed an ongoing project concerning a broad investigation of the discovery potential of instanton processes at the LHC. A final part of this review was devoted to our work on small-x saturation from an instanton perspective. After summarizing the considerable motivation for the relevance of instantons in this regime, the emerging intuitive, geometrical picture was illustrated with the simplest example, where indeed, saturation does occur. The form of the dipole cross section depends on the relation of two competing areas: the area $\pi\, r^2$, subtended by the $\bar{q}q$-dipole, and the area $\pi\, \langle\rho\rangle^2$ associated with the average size, $\langle\rho\rangle \approx 0.5$ fm, of the background instanton. For $r/\langle\rho\rangle \ll 1$, the dipole cross section is dominated by the dipole area, corresponding to 'color transparency'. For $r/\langle\rho\rangle \gtrsim 1$ it saturates towards a constant proportional to the background instanton area. Correspondingly, the average I-size scale $\langle\rho\rangle$ is associated with the saturation scale. A further central and intriguing result concerned the identification of the Color Glass Condensate with the QCD-sphaleron state. Throughout, the non-perturbative information from lattice simulations was instrumental.

References

[1] A. Belavin, A. Polyakov, A. Schwarz and Yu. Tyupkin, Phys. Lett. **B 59**, 85 (1975).

[2] G. 't Hooft, Phys. Rev. Lett. **37**, 8 (1976); Phys. Rev. **D 14**, 3432 (1976); Phys. Rev. **D 18**, 2199 (1978) (Erratum).

[3] T. Schäfer and E. Shuryak, Rev. Mod. Phys. **70**, 323 (1998) and references cited therein.

[4] M.-C. Chu et al.,(**Phys. Rev. D**,) (49)60391994.

[5] A. Ringwald and F. Schrempp, *Proc. Quarks '94*, ed. D.Yu. Grigoriev et al. (Singapore: World Scientific) p. 170.

[6] S. Moch, A. Ringwald and F. Schrempp, Nucl. Phys. **B 507**, 134 (1997).

[7] A. Ringwald and F. Schrempp, Phys. Lett. **B 438**, 217 (1998).

[8] A. Ringwald and F. Schrempp, Phys. Lett. **B 459**, 249 (1999).

[9] I. Balitsky and V. Braun, Phys. Lett. **B 314**, 237 (1993).

[10] A. Ringwald and F. Schrempp, Comput. Phys. Commun. **132**, 267 (2000).

[11] T. Carli, J. Gerigk, A. Ringwald and F. Schrempp, *Proc. Monte Carlo Generators for HERA Physics (DESY-PROC-1999-02)* ed. A.T. Doyle et al. (Hamburg: DESY) p. 329.

[12] A. Ringwald and F. Schrempp, Phys. Lett. **B 503**, 331 (2001).

[13] D.A. Smith and M.J. Teper (UKQCD Collab.), Phys. Rev. **D 58**, 014505 (1998).

[14] D. Ostrovsky and E. Shuryak, Phys. Rev. **D 71**, 014037 (2005).

[15] H1 Coll., C. Adloff et al., Eur. Phys. J. **C 25**, 495 (2002).

[16] ZEUS Coll., S. Chekanov et al., Eur. Phys. J. **C 34**, 255 (2004).

[17] M. Petermann, PhD Thesis in preparation; M. Petermann and F. Schrempp, in preparation.

[18] F. Schrempp, J. Phys. **G 28**, 915 (2002).

[19] F. Schrempp and A. Utermann, Acta Phys. Polon. **B 33**, 3633 (2002).

[20] F. Schrempp and A. Utermann, Phys. Lett. **B 543**, 197 (2002).

[21] F. Schrempp and A. Utermann, *Proc. Strong and Electroweak Matter 2002*, Heidelberg, Oct. 2002, ed. M.G. Schmidt, p. 477 [arXiv:hep-ph/0301177].

[22] E. Iancu, A. Leonidov and L. D. McLerran, Nucl. Phys. **A 692**, 583 (2001);

E. Ferreiro *et al.*, Nucl. Phys. **A 703**, 489 (2002).

[23] F. R. Klinkhamer and N. S. Manton, Phys. Rev. **D 30**, 2212 (1984).

[24] E. V. Shuryak and I. Zahed, Phys. Rev. **D 69**, 014011 (2004).

[25] A. Yung, Nucl. Phys. **B 297**, 47 (1988).

[26] V.V. Khoze and A. Ringwald, Phys. Lett. **B 259**, 106 (1991).

[27] J. Verbaarschot, Nucl. Phys. **B 362**, 33 (1991).

[28] C. Bernard, Phys. Rev. **D 19**, 3013 (1979).

[29] S. Capitani, M. Lüscher, R. Sommer and H. Wittig, Nucl. Phys. **B 544**, 669 (1999).

[30] H1 Coll., C. Adloff et al., Eur. Phys. J. **C 21**, 33 (2001);
ZEUS Coll., S. Chekanov et al., Eur. Phys. J. **C 21**, 443 (2001).

[31] V.N. Gribov and L.N. Lipatov, Sov. J. Nucl. Phys. **15**, 438 (1972); L.N. Lipatov, Sov. J. Nucl. Phys. **20**, 94 (1975); G. Altarelli and G. Parisi, Nucl. Phys. **B 126**, 298 (1977); Y.L. Dokshitzer, Sov. Phys. JETP **46**, 641 (1977).

[32] A. De Rujula et al., Phys. Rev. **D 10**, 1649 (1974).

[33] L.N. Lipatov, Sov. J. Nucl. Phys. **23**, 338 (1976); V.S. Fadin, E.A. Kuraev and L.N. Lipatov, Phys. Lett. **B 60**, 50 (1975), Sov. Phys. JETP **44**, 443 (1976), Sov. Phys. JETP **45**, 199 (1977);
I.I. Balitsky and L.N. Lipatov, Sov. J. Nucl. Phys. **28**, 822 (1978).

[34] L.V. Gribov, E.M. Levin and M.G. Ryskin, Nucl. Phys. **B 188**, 555 (1981); L.V. Gribov, E.M. Levin and M.G. Ryskin, Phys. Rept. **100**, 1 (1983).

[35] D.M. Ostrovsky et al., Phys. Rev. **D 66**, 036004 (2002).

[36] H. Aoyama and H. Goldberg, Phys. Lett. **B 188**, 506 (1987); A. Ringwald, Nucl. Phys. **B 330**, 1 (1990); O. Espinosa, Nucl. Phys. **B 343**, 310 (1990).

[37] D. Diakonov and V. Petrov, Phys. Rev. **D 50**, 266 (1994).

[38] N. Nikolaev and B.G. Zakharov, Z. Phys. **C 49**, 607 (1990); Z. Phys. **C 53**, 331 (1992); A.H. Mueller, Nucl. Phys. **B 415**, 373 (1994).

[39] A.H. Mueller, *Parton Saturation - An Overview*, hep-ph/0111244, in *QCD Perspectives on Hot and Dense Matter*, NATO Science Series, Kluwer, 2002.

[40] F. E. Low, Phys. Rev. **D 12**, 163 (1975);
L. Frankfurt, G.A. Miller and M. Strikman, Phys. Lett. **B 304**, 1 (1993).

[41] K. Golec-Biernat and M. Wüsthoff, Phys. Rev. **D 59**, 014017 (1999); Phys. Rev. **D 60**, 114023 (1999).

[42] F. Bezrukov, D. Levkov, C. Rebbi, V. Rubakov and P. Tinyakov, Phys. Rev. **D 68**, 036005 (2003)

[43] A. Ringwald, Phys. Lett. **B 555**, 227 (2003); arXiv:hep-ph/0302112.